JCTC Journal of Chemical Theory and Computation

Article

pubs.acs.org/JCTC

Open Access on 03/18/2015

# Revisiting $H_2O$ Nucleation around $Au^+$ and $Hg^{2+}$: The Peculiar "Pseudo-Soft" Character of the Gold Cation

Robin Chaudret,[†,‡,§,⊥] Julia Contreras-Garcia,[†,‡] Mickaël Delcey,[†,‡,∥] Olivier Parisel,[†,‡] Weitao Yang,[§] and Jean-Philip Piquemal*[,†,‡]

[†]Sorbonne Universités, UPMC Univ Paris 06, UMR 7616, Laboratoire de Chimie Théorique, case courrier 137, 4 place Jussieu, F-75005, Paris, France

[‡]CNRS, UMR 7616, Laboratoire de Chimie Théorique, case courrier 137, 4 place Jussieu, F-75005, Paris, France

[§]Department of Chemistry, Duke University, Durham, North Carolina 27708, United States

[∥]Department of Chemistry − Uppsala University, Ångström Laboratory, Theoretical Chemistry, Ångströmlaboratoriet Lägerhyddsvägen 1751 20 Uppsala, Sweden

Supporting Information

**ABSTRACT:** In this contribution, we propose a deeper understanding of the electronic effects affecting the nucleation of water around the $Au^+$ and $Hg^{2+}$ metal cations using quantum chemistry. To do so, and in order to go beyond usual energetical studies, we make extensive use of state of the art quantum interpretative techniques combining ELF/NCI/QTAIM/EDA computations to capture all ranges of interactions stabilizing the well characterized microhydrated structures. The Electron Localization Function (ELF) topological analysis reveals the peculiar role of the Au+ outer-shell core electrons (subvalence) that appear already spatially preorganized once the addition of the first water molecule occurs. Thus, despite the addition of other water molecules, the electronic structure of $Au(H_2O)^+$ appears frozen due to relativistic effects leading to a maximal acceptation of only two waters in gold's first hydration shell. As the values of the QTAIM (Quantum Theory of Atoms in Molecules) cations's charge is discussed, the Non Covalent Interactions (NCI) analysis showed that $Au^+$ appears still able to interact through longer range van der Waals interaction with the third or fourth hydration shell water molecules. As these types of interaction are not characteristic of either a hard or soft metal cation, we introduced the concept of a "pseudo-soft" cation to define $Au^+$ behavior. Then, extending the study, we performed the same computations replacing $Au^+$ with $Hg^{2+}$, an isoelectronic cation. If $Hg^{2+}$ behaves like $Au^+$ for small water clusters, a topological, geometrical, and energetical transition appears when the number of water molecules increases. Regarding the HSAB theory, this transition is characteristic of a shift of $Hg^{2+}$ from a pseudosoft form to a soft ion and appears to be due to a competition between the relativistic and correlation effects. Indeed, if relativistic effects are predominant, then mercury will behave like gold and have a similar subvalence/geometry; otherwise when correlation effects are predominant, $Hg^{2+}$ behaves like a soft cation.

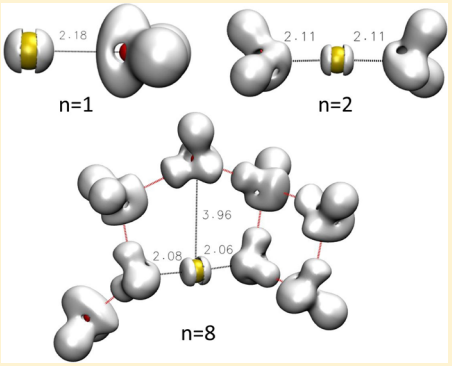


## 1. INTRODUCTION

Initially restricted to atmospheric experimental studies,[1] the study of water nucleation, namely the condensation of water molecules around charged particles, has been extended in recent years to the study of $M^{p+}$ metal cations microhydration[2] in clusters. Indeed understanding the bonding properties of a metal cation within its first hydration shell or the organization of the solvent molecules around the cation in ($[M(H_2O)_n]^{p+}$) clusters can help to identify their selectivity and to understand their involvement in complex biological (i.e., metal poisoning[3]) and chemical (catalytic capacities[4]) processes. In this line, experiments have been shown to be able to describe the nucleation of water molecules around heavy metals such as gold thanks to Collision Induced Dissociation (CID) techniques.[5] For quantum chemists, such systems have been highly challenging for several decades[6a] as they raise the double problem of the inclusion of both the electronic correlation and relativity effects within electronic structure computations (see refs 6b−d and references therein).

From this perspective, electronic structure studies are divided into two categories: on the one hand, high level gas phase quantum calculation, with accurate treatment of the relativistic and correlation effects, on small size clusters,[6−16] and on the other hand solvated cations treated at a hybrid Quantum Mechanics/Molecular Mechanics (QM/MM) level to obtain condensed phase results.[17−19] In both cases, several experimental results allowed the validation of those theoretical results.[5,20−23]

**Received:** July 12, 2013
**Published:** March 18, 2014

  

Moreover, to understand the intrinsic importance of local quantum effects due to the metals, a new theoretical "interpretative" strategy has been applied through the use of Quantum Chemical Topological (QCT) analyses. Indeed, de Courcy et al.[24] showed that the Electron Localization Function[25,26] (ELF) topological analysis could define a topological criterion to discriminate hard and soft metal cations in their local environment providing new insights about physical phenomena at play. Thus, a soft (polarizable) cation is able to split/delocalize its outer-shell core density (denoted as core subvalence) into different space domains (basins) in order to accommodate the perturbing environment (induction-like effects). On the contrary, the electronic density of a hard (and poorly polarizable) cation remains spherical under the same circumstances. Such effects have been shown to be directly linked with observed increases of second order metal energies such as polarization and charge transfer (induction terms) in energy decomposition analysis approaches.

In this contribution, we intend to follow up on theoretical studies[6−8,10] devoted to gold in order to more deeply understand the physical effects at play in water nucleation around it and to extend it by comparing such microsolvation to $Hg^{2+}$ which is isoelectronic to $Au^{+}$. Indeed, it should allow us to illustrate the importance of the electronic correlation vs relativity competition having in mind that if relativity is more important for gold than for any other sixth row[6] cations, $Hg^{2+}$ should nevertheless exhibit smaller but noticeable relativistic effects.

To do so, we will study the water molecules nucleation around these two metal cations at a quantum mechanical level in clusters encompassing a number of water molecules ranging from 1 to 16 (denoted $[M(H_2O)_n]^{p+}$ or $[M]_n$ where M is the metal name (i.e., Au or Hg), $n$ is the number of water molecules in the complex, and $p$ is the charge of the complex ($p$ = 1 for Au and 2 for Hg)). In order to provide further insights into the bonding properties of gold and mercury cations and techniques to go beyond usual energetical studies, we will make extensive use of quantum interpretative techniques such as ELF or an energy decomposition analysis (EDA) scheme such as the Constrained Space Orbital Variations (CSOV) approach.[27] We will also use the newly developed Non-Covalent Interaction (NCI) method[28,29] to unravel weak interactions in clusters and quantify their strength. Overall, each one of the obtained structures will be submitted to a full cross-interpretative analysis scheme using combined analyses.

## 2. THEORETICAL AND COMPUTATIONAL METHODS

**Computational Details.** *Molecular Geometries.* For $Au^{+}$ and $Hg^{2+}$ water complexes, Gaussian 09[30] geometry optimizations were performed using Density Functional Theory (DFT) at a B3LYP/6-31+G**[31−33] level on water molecules and using the SDD[34] pseudopotentials for the metal cations. Such a pseudopotential was found to give consistent results for the $[Au(H_2O)]^{+}$ complex in comparison with full electron, relativistic calculations using a four-component Hamiltonian[11] that cannot be performed on the presently studied large systems. Table 1 provides a short comparison of the agreement between scalar treatment using SDD pseudopotentials and all-electrons fully relativistic (four-component) results. Moreover, it is important to point out that topological analyses such as ELF/QTAIM/NCI require to have access to the relaxed electron density. The present choice is therefore completely relevant for such an analysis.

**Table 1. Geometrical Parameters (Å and Degrees) and Complexation Energy (kcal/mol) for the $[Au(H_2O)]^{2+}$ and $[Hg(H_2O)]^{2+}$ Complexes at the 6-31+G**/SDD/B3LYP and All Electrons (AE)/DB3LYP 4-Component Levels (See Details in Ref 11)**

| cation | $[Au(H_2O)]^{+}$ | | $[Hg(H_2O)]^{+}$ | |
|---|---|---|---|---|
| method | B3LYP/SDD | DB3LYP/AE | B3LYP/SDD | DB3LYP/AE |
| $r$(M−O) | 2.177 | 2.137 | 2.150 | 2.112 |
| $r$(O−H) | 0.972 | 0.972 | 0.989 | 0.989 |
| $B$(HOH) | 108.3 | 109.0 | 109.2 | 109.6 |
| $\Delta E$ | −38.7 | −41.2 | −93.7 | −95.6 |

All optimized structures were characterized by a full vibrational analysis as frequencies were calculated for each one of the optimized geometries so as to ensure that the finally obtained geometry was at least a local minimum.

For gold, the initial structures were built upon ones proposed by Reveles et al.[7] In addition, different starting geometries were tested, such as octahedral geometries. For mercury, we choose our gold optimized structures as guess geometries, but other initial geometries were also considered.

For mercury, additional computations were performed. Indeed, for the $[Hg(H_2O)_3]^{2+}$ complex, different DFT functionals such as BLYP, PBE0,[35] PW91PW91,[36] and ab initio methods such as HF, MP2, CCSD, and CCSD-T, as well as various basis sets (6-31+G**,[33] 6-311++G**,[37] aug-cc-pVDZ,[38] aug-cc-pVTZ[38]) were tested. Several treatments of the relativistic effects including scalar SDD pseudopotential and different levels of Douglas−Kroll theory[39−41] were used to assess the validity of our calculation. Full Douglas−Kroll/aug-cc-pvtz computations were performed for clusters up to seven water molecules. We also studied the competition between the linear and centered form of mercury complexed with three ligands $[Hg(X)_3]^{+2-p}$, X = HF, $NH_3$, imidazole, $NH_2^-$, $H_2O$, $OH^-$, $H_2S$, $HS^-$, and $CH_3S^-$ and $p$ being their respective charge. For these systems, calculations were performed at the B3LYP/SDD/6-31+G** level of theory. The different ligands were chosen to be ranked from typically hard (HF) to typically soft ($CH_3S^-$) ligands.

*Charge Analysis.* To compare to previous studies, various charge analysis schemes have been used in order to discuss the evolution (and stability) of the metal cation's charge as a function of the number of water molecules of the complexes.

The Mulliken,[42] Natural Bond Orbital[43,44] (NBO), and Atoms In Molecules[45,46] (QTAIM) charges were performed. Mulliken and NBO analyses were performed using Gaussian. The Top_Mod[47] software was used for all QTAIM computations as well as for the distributed moment analysis based on the QTAIM partition.[48,49] To study the effects of the method/basis set choices, charges were also computed on the previously optimized structures using other levels of theory: MP2, HF, BLYP, B3LYP, PBE0, PW91PW91, and M06-2X[50]—and using other basis sets: STO-3G,[51] 3-21G,[52] DZVP,[53] 6-31+G**,[33] 6-31++G**,[33] 6-311++G**,[37] and aug-cc-pVTZ.[38] The basis sets range from minimal to double or triple-$\zeta$ basis sets with diffuse and polarization orbitals. The DZVP basis set was additionally used in order to compare our results with those from Reveles et al.[7]

**Quantum Chemical Topology (QCT) Approaches.** *a. The ELF Topological Analysis.* The ELF function was originally studied by Becke and Edgecombe.[25] It was later associated with a measure of the Pauli repulsion in the atomic


dx.doi.org/10.1021/ct4006135 | J. Chem. Theory Comput. 2014, 10, 1900−1909

or molecular space by Silvi and Savin.[26] It also enables access to the probability of finding two same spin electrons. ELF values are restricted between 0 and 1 and can be interpreted as a signature of the electronic pair distribution, but in contrast to pair functions, it can be easily calculated and interpreted. The ELF function can be partitioned into an intuitive chemical scheme once it has been computed on a 3D grid from a given ab initio method. Indeed, core regions, denoted C(X), can be determined for any atom. This is also the case for valence regions associated with lone pairs, denoted V(X), and for chemical bonds [V(X,Y)]. These ELF regions, called basins (denoted as X), match closely the domains of Gillespie and Nyholm's valence shell electron pair repulsion model.[54] All computations were performed using the Top_Mod package.[47]

**Subvalence and Electronic Localization Function.** In a recent study, de Courcy et al.[24] showed that some metal cations were able to split their inner shell core electron density (named subvalence) in order to accommodate to the environment (see Figure 1). They also realized that the ability of a cation to split

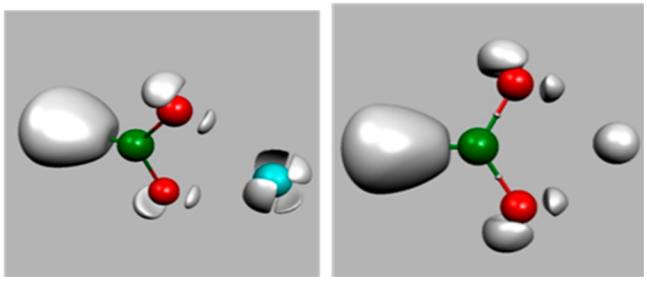

**Figure 1.** ELF topology of a soft cation such as $Ca^{2+}$ that splits its outer-shell density into subvalence domains vs a hard cation such as $Mg^{2+}$ that remains spherical.

its subvalence was directly related to its hardness/softness properties: indeed, hard cations never split their subvalence whereas soft cations ones are able to split it. Such a property was also demonstrated to have an important implication in biomolecular systems such as enzymes.[55,56]

In addition to the usual topological analysis, it is possible to use ELF theory to obtain properties such as the partial charge or the different first moments integrated on the ELF basin.[49] As the equations are very general, these properties can also be integrated on the QTAIM basins so as to obtain the atomic partial charges or first moments.

*b. The NCI Analysis.* Recently, Johnson et al. introduced the reduced density gradient as a new scalar function able to analyze noncovalent interactions,[28,29] providing a rich representation of van der Waals interactions, hydrogen bonds, and steric repulsions. Such a function is defined using the electron density and its first derivatives:

$$s(\rho) = \frac{1}{2(3\pi^2)^{1/3}} \frac{|\nabla\rho|}{\rho^{4/3}}$$

It is a dimensionless quantity used in DFT to describe the deviation from a homogeneous electron distribution. In density tails (i.e., regions far from the molecule, in which the density is decaying to zero exponentially), the reduced gradient has very large positive values. On the contrary, the $s(\rho)$ function assumes values approaching zero for regions of both covalent bonding and noncovalent interactions.

These low $s(\rho)$ areas are traced back to molecular space that gives rise to isosurfaces, enabling the visualization of the weak interactions of the system. In order to differentiate between the different types of interactions, we will use the following color code:

- Blue for the highly attractive weak interactions (such as hydrogen bonds)
- Green for the extremely weak interactions (such as dispersive-like van der Waals)
- Red for repulsive interactions (such as steric clashes)

*c. Combined ELF/NCI Analysis.* The synergetic use of ELF and NCI[57] enables the simultaneously identification of regions of strong and weak electron pairing. Initially devoted to the study and the understanding of chemical reaction mechanisms,[57] it has been recently applied to the understanding of the role of metal for metalloenzymes reactivity.[56]

**Energy Decomposition Analysis (EDA).** The interaction energy between two or more fragments such as a cation and its ligands can be decomposed into four different contributions:

$$\Delta E = E_C + E_{exch/rep} + E_{pol} + E_{CT}$$

namely, Coulomb/electrostatic energy ($E_C$), short-range exchange-repulsion energy ($E_{exch/rep}$) in first-order ($E_1$ is the sum of $E_C$ and $E_{exch/rep}$ energies), polarization energy ($E_{pol}$), and charge-transfer energy ($E_{CT}$) in second-order ($E_2$ is the sum of the $E_{pol}$ and $E_{ct}$ energies, sometimes denoted as induction). All of these four terms can only be computed at the DFT level with the B3LYP functional using the Constrained Space Orbital Variations (CSOV)[27,58a] procedure in a modified version of the HONDO 95.3 software.[59] Such a procedure has been shown to be fully applicable to heavy metals.[58] Computations were performed on both gold and mercury complexes for clusters $[M]_n$ $n$ = 2 to 16 and M being Au or Hg. Table 2 shows the evolution of the polarization and charge transfer energies (kcal/mol) for $[Au]_n$.

**Table 2. Evolution of the Polarization and Charge Transfer Energies (kcal/mol) for $[Au]_n$ ($n$ = 2 to 10) at the 6-31+G**/SDD/B3LYP Level**

| decomposition | polarization (kcal/mol) | | charge transfer (kcal/mol) | |
|---|---|---|---|---|
| complex | cation | water | water to cation | cation to water |
| $[Au(H_2O)_2]^+$ | −25.7 | −21.0 | −37.8 | −3.2 |
| $[Au(H_2O)_3]^+$ | −28.5 | −23.4 | −41.4 | −3.4 |
| $[Au(H_2O)_4]^+$ | −31.7 | −25.1 | −43.2 | −3.5 |
| $[Au(H_2O)_5]^+$ | −33.9 | −27.5 | −47.2 | −3.4 |
| $[Au(H_2O)_6]^+$ | −35.7 | −29.1 | −48.6 | −3.5 |
| $[Au(H_2O)_7]^+$ | −34.0 | −28.6 | −48.0 | −3.4 |
| $[Au(H_2O)_8]^+$ | −35.4 | −30.5 | −50.1 | −3.4 |
| $[Au(H_2O)_9]^+$ | −33.1 | −29.5 | −47.4 | −3.4 |
| $[Au(H_2O)_{10}]^+$ | −33.6 | −30.9 | −48.8 | −3.3 |

## 3. THEORETICAL STUDY OF WATER MOLECULE NUCLEATION AROUND $AU^+$: RESULTS AND DISCUSSION

In this section, we will first present the computed structures and discuss their significance compared to previous experimental and theoretical studies. We will then apply an extensive multimethod strategy using various quantum interpretative techniques in order to deeper study the present electronic

effects. Finally, we will discuss the final charge on the $Au^+$ cation within the complexes.

**Structures and Energies of $[Au]_n$ Complexes.** The Basis Set Superposition Error (BSSE) and Zero Point Energy (ZPE) corrected incremental binding energy of a cluster ($[Au]_n$ for example) can be defined as the difference between the bonding energy of the $[Au]_n$ and the $[Au]_{n-1}$ complexes. It therefore represents the change in energy due to the bonding of the water number $n$.

For the gold cation, we compared our incremental bonding energies to other studies including reference experimental gas phase bonding energies (Poisson et al.[5]) and theoretical works (Lee et al.,[60] Feller et al.,[10] Reveles et al.[7]) as shown in Figure 2.

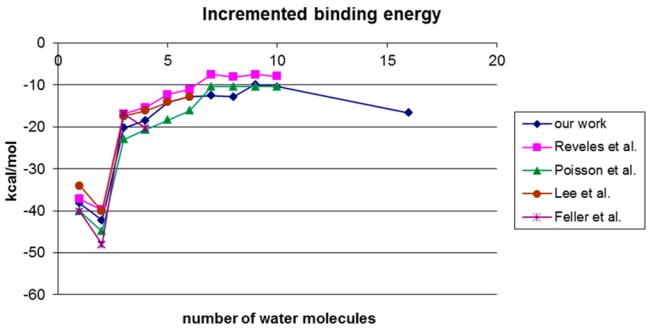


**Figure 2.** BSSE/ZPE corrected incremented bond energy (in kcal $mol^{-1}$) for increasing the size of clusters from our study (diamonds) or other experimental (triangles, points and stars) as well as theoretical results (squares).

They all reported that the two first water molecule additions were at least twice as favorable (around 35 to 45 kcal/mol) as the following ones (from 10 to 20 kcal/mol). The second water molecule appears more strongly bound than the first one. This specificity of the gold cation has been attributed to the large relativistic effects it undergoes.[6b−d,11] As shown in Figure 2, our results agree with these previous studies and therefore state that our optimized structures can be assimilated as reasonable global minima.

For ($[Au(H_2O)_2]^+$) and larger clusters, only two water molecules remain linearly bonded to the cation with an angle ranking between 170° and 178°, the others being located in the second and third hydration shells. For medium size clusters (up to $[Au]_7$), hydrogen bonded water molecules attempt to form rings on each side of the cation. For the largest clusters (eight or more water molecules), some water molecules are bridging the two sides of the cation thanks to hydrogen bonds. They are however localized too far from the cation (around 4 Å instead of 2 Å for the first solvation water molecules) to be considered bonded to it.

**Cross Interpretative Analysis of the Interaction between $Au^+$ and Its Environment: Notion of Pseudo-soft Cation and Study of the Au−O Bond.** The ELF topological analysis shows that gold's subvalence is divided into two half-sphere domains pointing along the Au−O bond (Figure 3 and Figure S1 in Supporting Information for larger images of all the complexes). This subvalence is conserved whatever the number of water molecules is, i.e., from 1 to 16 water molecules. Indeed, it is already preorganized at the one water molecule stage and will not be modified even with the apparition of bridging water molecules and can be therefore considered as frozen. This preorganization can be traced back

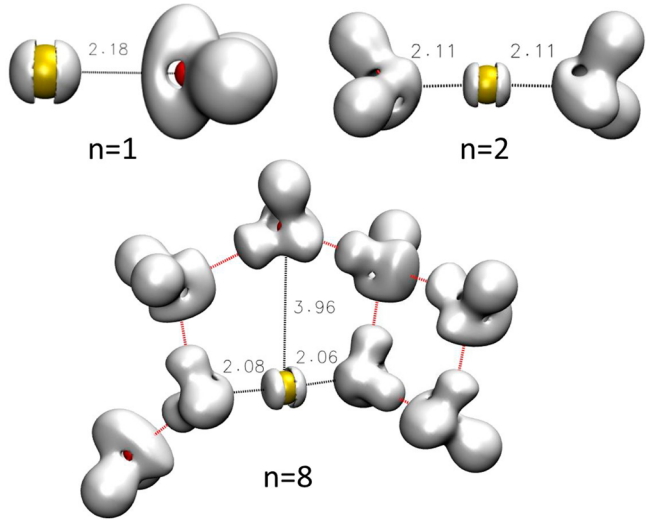


**Figure 3.** ELF isosurfaces (ELF = 0.78) for different $[Au]_n$ ($n$ = 1, 2, and 8) clusters. For each of them, the distance between the closest water molecules and the cation are added (Å). For a better visibility, the pictures of the other complexes studied can be found in Figure S1 in the Supporting Information. All structures were computed at the B3LYP/SDD/6-31+G** level of theory.

to the importance of relativity which was shown to dominate the $Au(H_2O)^+$ complex (see ref 11 for the importance of relativity vs correlation effects using all-electrons-DFT 4-components computations). This last part reinforces the fact that $Au^+$ only strongly interacts with the two first hydration shell water molecules (in agreement with Pyykkö et al.[6d] who proposed results in that direction).

For small clusters, NCI and ELF give very similar results, as interactions between the cation and the two first hydration shell water molecules can be found (Figure 4 and Figure S2 in the Supporting Information for larger images of all the complexes). For clusters of eight and more water molecules, however, differences arise as weak interactions can be found between the bridging water molecules and the cation. These interactions are

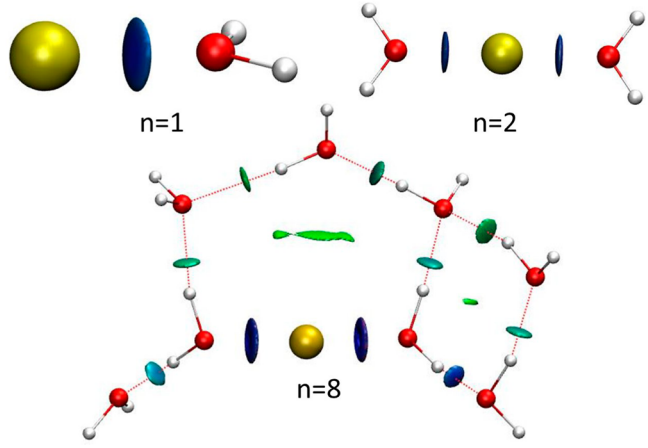


**Figure 4.** NCI analysis for several $[Au]_n$ ($n$ = 1, 2, and 8) complexes. The colors range from blue for strongly attractive interactions to red for repulsive ones. For more visibility, the pictures of all the complexes studied can be found in Figure S2 in the Supporting Information. All structures were computed at the B3LYP/SDD/6-31+G** level of theory.


dx.doi.org/10.1021/ct4006135 | J. Chem. Theory Comput. 2014, 10, 1900−1909

weak (van der Waals strength type) as the density value associated is very small. The NCI approach also explains the reason why cycles are formed between hydrogen bonded water molecules. Indeed, an attractive interaction domain can be found in the center of those cycles of four water molecules that corresponds to an additional stabilization due to their formation. NCI analyses on $MP_2$ single point relaxed densities on DFT structures displayed the same picture.

Finally, regarding the definition of hardness/softness introduced by de Courcy et al.,[24] $Au^+$ cannot be considered as a hard cation as it splits its subvalence into two half-spheres, but neither can it be considered as a soft cation as once its subvalence is split into two domains, the cation is strongly polarized by the water molecules. Moreover, it is important to note that $Au^+$ appears impervious to any change in the external field that is a characteristic of a hard cation. It will therefore be designated as a "pseudo-soft" cation.

We mentioned previously that the strength of the two Au−O bonds was very important (35 to 45 kcal/mol, see Figure 2). The ELF analysis shows that an electron donation from the ligand to the subvalence basins of the metal exists (for example 0.06 $e^-$ for the $[Au]_4$ complex). Back donation from the metal into first solvation shell oxygen water lone pairs also takes place in these systems (0.05 $e^-$ out of 1.63 and 0.05 $e^-$ out of 1.65 in the $[Au]_4$ complex). To investigate it further, we performed decomposition analysis on the different $[Au]_n$, $n$ = 2 to 10, complexes. Using CSOV energy decomposition, we found important charge transfer energies from the water molecules to the cation and also from the cation to the water molecules (see results in Table 3), which is in agreement with the ELF results.

**Table 3. Evolution of the Population ($q$) and of the First ($M_1$) and Second ($M_2$) Moments (in a.u.) of the Mercury for the Clusters $[Hg]_n$ ($n$ = 2 to 16)**

| complex | $q$ | $M_1$ | $M_2$ |
|---|---|---|---|
| $[Hg]_2$ | 1.4 | 0.07 | 1.95 |
| $[Hg]_3$ | 1.4 | 0.07 | 2.41 |
| $[Hg]_4$ | 1.4 | 0.08 | 2.59 |
| $[Hg]_5$ | 1.3 | 0.07 | 2.51 |
| $[Hg]_6$ | 1.3 | 0.07 | 2.55 |
| $[Hg]_7$ | 1.3 | 0.13 | 2.88 |
| $[Hg]_8$ | 1.3 | 0.12 | 3.21 |
| $[Hg]_9$ | 1.2 | 0.33 | 2.65 |
| $[Hg]_{10}$ | 1.4 | 0.27 | 1.38 |
| $[Hg]_{16}$ | 1.4 | 0.06 | 0.57 |

Therefore, the Au−O bond appears as a very strong metal ligand bond due to its partial covalence that mixes metal and ligand electrons.

Finally, both polarization and charge transfer energies appear stable whatever the number of additional water molecules. This suggests that the remaining interactions between the cation and its ligand (especially for bridging complexes) are mainly due to other effects such as electrostatics or dispersion.

**Study of the Charge Sensitivity to Methodology.** In a previous study, Reveles et al.[7] computed the evolution of gold Mulliken charge as a function of the number of water molecules of the complexes. They concluded that gold's charge could decrease so much with the number of water molecules that the cation finally appeared almost neutral (charge less than +0.10 $e^-$ for $[Au]_n$, $n \geq 5$). However, in agreement with Lee et al.,[60] they also showed that such a phenomenon was more a trend than an actual neutralization of the gold cation, as other charge analysis schemes such as NBO were finding far less electron transfer to $Au^+$. We propose here a detailed analysis of the influence of the methodology on the gold charge. In agreement with Reveles et al., we show similar trends as $Au^+$ exhibits the capability to partially recover an electronic fraction. However, our QTAIM population analysis clearly shows that the $Au^+$ charge never decreases beyond +0.6 $e^-$, preventing any full neutralization of the gold cation.

We therefore decided to investigate more precisely the role of the charge population analysis approach, the basis set, and the ab initio computational method used.

NBO, QTAIM, and Mulliken population analysis were performed for all complexes with cluster encompassing up to 10 water molecules ($[Au]_n$, $n$ = 1 to 10). The B3LYP functional was used together with the 6-31+G** basis set on the water molecules and the SDD pseudopotential on gold. QTAIM and NBO analyses give relatively similar results showing a gold charge that never decreases below +0.6 $e^-$ (as shown in Figure 5a and Figure S3-a), whereas the Mulliken population, on the contrary, decreases up to +0.4 $e^-$. This difference between Mulliken and NBO charges had already been noticed by Reveles et al. and arises from the well-known unstabilities of the Mulliken approach (see refs 45, 46, and 61, for discussion)

Indeed, as expected, the basis set has a strong influence on the results (see Figure 5b and Figure S3-b). It appears that the charge is stable for relatively large basis sets (at least DZVP or 6-31+G**), but very important variations can however be seen for small basis sets. For example, the use of a minimal basis set such as STO-3G will even lead to a negatively charged gold. Consequently, it seems mandatory to use, at least, a double-$\zeta$ with polarization and diffuse functions basis sets to accurately model such systems to avoid an unphysical description of the electronic structure.

Finally, we investigated the influence of the ab initio or DFT computational approach on the gold population analysis. Figure 5c (and Figure S3-c) sums up the results. The cation charge is slightly modified with the ab initio or DFT method used. If we compare to the MP2 charges, HF ones appear always too important, whereas DFT ones are usually smaller. The HF approach seems therefore to underestimate the delocalization of the gold charge. When, on the contrary, DFT methods overestimate it. These results are in good agreement with the delocalization error described in refs 58, 62, and 63.

In addition, it is interesting to notice that all the hybrid functionals reproduce better MP2 charges probably due to the addition of a part of exact HF exchange. Among the others, the M06-2X charges remain closest to the MP2 ones. Finally, our results are also in good agreement with the fact that the DFT delocalization error is decreasing with the size of the cluster while the HF one is not.[62,63]

Overall, all the results gathered here show that the charge of gold is method- and basis-dependent, as could have been anticipated. Moreover, it seems necessary to use NBO or QTAIM population analysis with hybrid DFT calculation and a basis set larger or equal to DZVP. Nevertheless, if $Au^+$ tends to recover a fraction of an electron, it seems far from an actual neutralization of its +1 charge that was discussed by Reveles et al.[7]

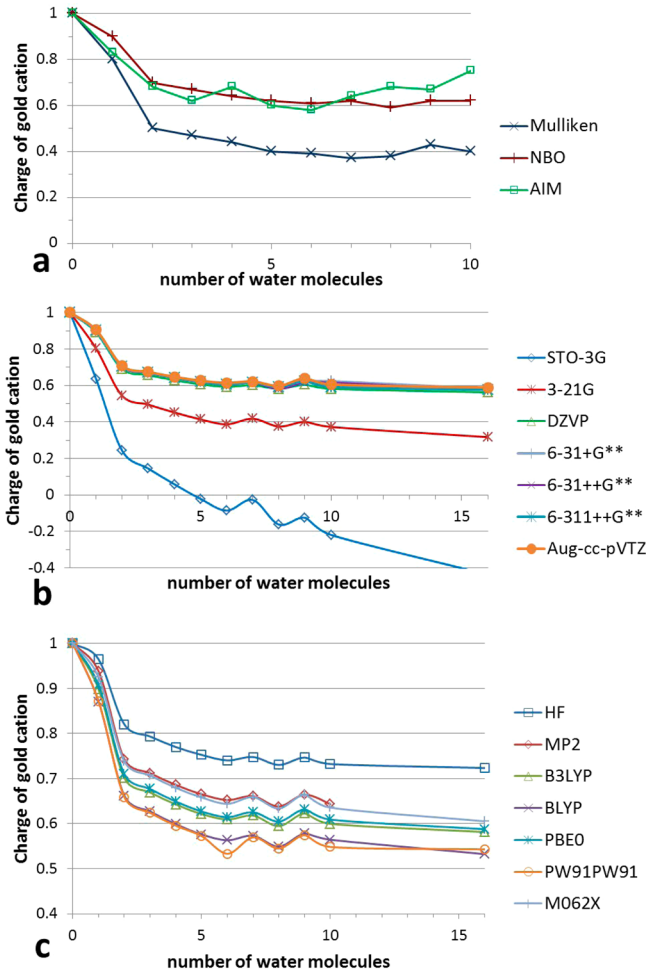


**Figure 5.** Evolutions of gold charge for different $[Au]_n$ clusters: (a) NBO, QTAIM, and Mulliken population analysis (in $e^-$) for $[Au]_n$ $n$ = 1, 10 clusters computed at the B3LYP/SDD/6-31+G** level of theory. (b) NBO charge for $[Au]_n$ complexes ($n$ = 1 to 16) using STO-3G, 3-21G, DZVP, 6-31+G**, 6-31++G**, 6-311++G**, and aug-cc-pVTZ. (c) NBO charge for the different $[Au]_n$ clusters ($n$ = 1 to 16) using HF, MP2, B3LYP, BLYP, PBE0, PW91PW91, and M06-2X. For more visibility, the pictures of the other complexes studied can be found in Figure S3 in the Supporting Information.

## 4. THEORETICAL STUDY OF WATER MOLECULE NUCLEATION AROUND $HG^{2+}$: RESULTS AND DISCUSSION

To complement our results and following the same computational protocol, we extended our water nucleation study to $Hg^{2+}$, which is isoelectronic to $Au^+$.

**Cross Interpretative Analysis of $[Hg]_n$ ($n$ = 1 to 16) Complexes.** For complexes with up to eight water molecules, the mercury behaves similarly to gold: it only bonds to two water molecules, with the remaining going to the second or third hydration shell. Its subvalence splits also into two half-spheres directed toward the Hg−O bond. Several differences do however arise. Indeed, the mercury cation deprotonates its first solvation shell water molecules. This property is eager to be due to the higher charge transfer and therefore more important covalent character of the Hg−O bonds (see Table 4). In order to reduce electrostatic repulsion, the created protons will then be transferred as far as possible from the cation. This induces a second difference as, in mercury, water molecules tend then to create hydrogen bonded water strings instead of rings in gold clusters.

**Table 4. Polarization and Charge Transfer Energies (in kcal/mol) for the Different $[Hg]_n$ ($n$ = 2 to 16) as Computed at B3LYP Level Using CSOV Procedure**

| decomposition | polarization (kcal/mol) | | charge transfer (kcal/mol) | |
|---|---|---|---|---|
| complex | cation | water | water to cation | cation to water |
| $[Hg]_2$ | −11.3 | −49.9 | −56.6 | −1.6 |
| $[Hg]_3$ | −14.8 | −64.7 | −70.0 | −1.8 |
| $[Hg]_4$ | −17.5 | −72.3 | −73.4 | −1.9 |
| $[Hg]_5$ | −18.1 | −74.3 | −73.4 | −1.9 |
| $[Hg]_6$ | −19.0 | −78.2 | −75.1 | −1.9 |
| $[Hg]_7$ | −19.9 | −85.1 | −83.8 | −2.0 |
| $[Hg]_8$ | −21.4 | −90.7 | −89.1 | −2.1 |
| $[Hg]_9$ | −17.1 | −95.5 | −78.1 | −1.5 |
| $[Hg]_{10}$ | −6.7 | −91.8 | −59.3 | −1.5 |
| $[Hg]_{16}$ | −2.7 | −121.1 | −54.9 | −1.1 |

For more than eight water molecules, the mercury switches from its "gold type" or "linear type" solvation to a "centered" one where $Hg^{2+}$ accepts more than two water molecules in its first solvation shell. This transition can be characterized looking at its ELF subvalence basins that move from the two half-spheres to a more divided form characteristic of soft cations (Figure 6 and Figure S4 in the Supporting Information for larger images of all the complexes). This topological transition explains why, for small clusters, the mercury has a gold type solvation structure, whereas once solvated, mercury binds seven water molecules.[20,21,64]

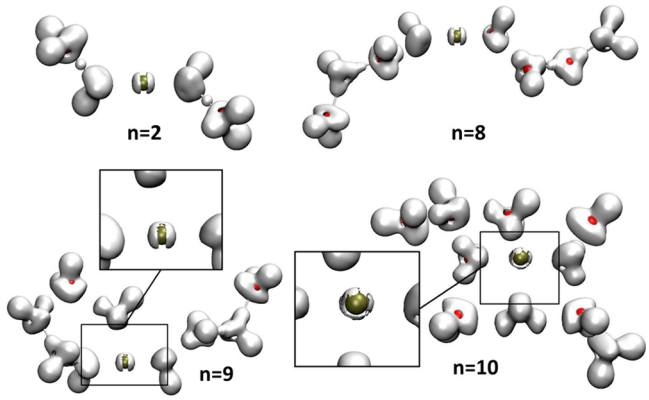


**Figure 6.** ELF representation (ELF = 0.775) for complexes $[Hg]_n$, $n$ = 4, 8, 9, or 10. Specific attention was paid to the subvalence domain of the cation for each cluster. For more visibility, the pictures of all the complexes studied can be found in Figure S4 in the Supporting Information. All structures were computed at the B3LYP/SDD/6-31+G** level of theory.

The NCI analysis (Figure 7 and Figure S5 in the Supporting Information for larger images of all the complexes) shows that Hg−O bond strength is decreasing when mercury accepts more than two water molecules in its first hydration shell. These modifications induce the loss of the mercury ability to deprotonate the water molecules. Indeed, as the bond gets weaker, the acidity gets smaller. Despite the increasing number of water molecules in its first hydration shell, the mercury still binds more strongly two opposed water molecules just as in smaller clusters (the angle O−Hg−O ranks between 148° and


dx.doi.org/10.1021/ct4006135 | J. Chem. Theory Comput. 2014, 10, 1900−1909

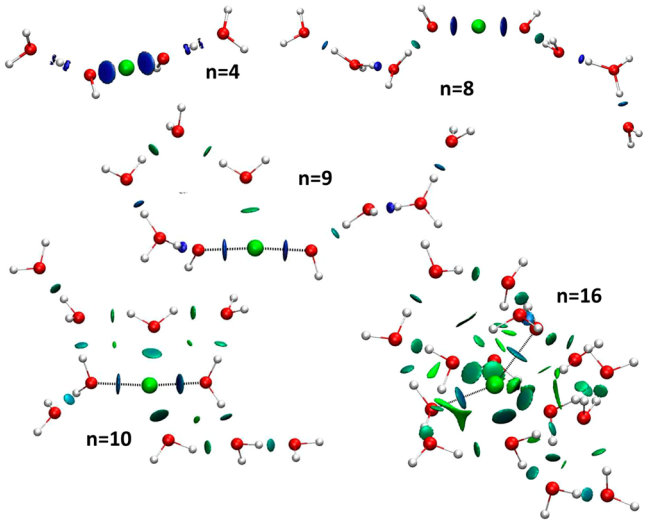


**Figure 7.** NCI analysis for several $[Hg]_n$ complexes ($n$ = 4, 8, 9, 10, 16). In $[Hg]_n$ complexes, only the two most important interactions between mercury and water molecules are represented. The colors range from blue for strongly attractive interactions to red for repulsive ones. For more visibility, the pictures of all the complexes studied can be found in Figure S5 in the Supporting Information. All structures were computed at the B3LYP/SDD/6-31+G** level of theory.

180°). Indeed, the density characteristic of these interactions is higher than those of other cation/water molecule interactions (for example, 0.063 and 0.061 compared to 0.049, 0.044, 0.040, and 0.028 in $[Hg]_{16}$). Therefore, even if its coordination increases, the mercury remains more strongly bonded to two water molecules presenting a "gold type" geometry.

In a previous paper, Cox and Stace[12] studied the reasons leading to the gas phase's unusual acidity of mercury on small hydrated clusters ($[Hg(H_2O)_2]^{2+}$ and $[Hg(H_2O)_4]^{2+}$). For these small complexes, our results are similar: they found that mercury was able to deprotonate bonded water molecules. This property was said to lead to its unusually important acidity in water. However, our calculations showed that, for large clusters ($[Hg]_n$ $n$ = 9, 10, and 16), the mercury loses this ability but remains more strongly bonded to two water molecules (as shown in NCI analysis). Therefore, $Hg^{2+}$ will enhance the acidity of these two water molecules, and it will consequently increase its solvated acidity.

The study of the QTAIM charge and a distributed moments analysis (first and second moments) on the mercury (the first moment is a dipolar level contribution as the second moment is related to the quadrupole on the cation) gives additional information about the topological transition (see Table 3). Although the charge analysis remains unchanged, the first and second moments, on the contrary, show important differences before and after the transition. Indeed, the first moment, which fluctuates between 0.07 and 0.13 au from one to eight water molecules, reaches 0.32 au for $[Hg]_9$ and then decreases to 0.06 au for $[Hg]_{16}$. The second moment increases slowly from 1.95 to 3.21 between $[Hg]_2$ and $[Hg]_8$ and starts decreasing rapidly after. It is finally divided by 6 between $[Hg]_8$ and $[Hg]_{16}$ water molecules due to the greater symmetry of the set.

The QTAIM moments ($M_1$ and $M_2$) appear therefore to be good descriptors of the topological transition, whereas a charge analysis would not have noticed any differences. It appears then important to look at higher moments than the charge that can provide information on more complex events.

Table 4 shows that the cation polarization increases up to −21.4 kcal/mol for $[Hg]_8$ but suddenly decreases for nine water molecules (−17.1 kcal/mol) and finishes divided by 10 for $[Hg]_{10}$ (−2.70 kcal $mol^{-1}$). This transition is also visible in the charge transfer energies from cation to water and from water to cation that are both divided by 2 when going from 8 to 10 water molecules. The polarization of the solvent keeps going up as it is not concerned by the transition.

The energy decomposition analysis shows also that charge transfer from the ligands to the cation is almost twice as important in mercury than in gold cations, whereas it is the contrary for the charge transfer from the cation to the ligand. This could be understood as an increase of the donation of the ligands in the cation orbitals going together with a decrease of the back-donation. Indeed, relativistic effects on gold induce a contraction of the gold empty 6s orbital and an expansion of the full 5d one. As these effects are less important in mercury than in gold, their consequences will be smaller too.

**Influence of the Level of Theory on the Transition: Competition between the Relativistic and Electronic Correlation Effects.** If previous four-component/B3LYP all electrons computations[11] clearly demonstrated a lower influence of relativity on the monoligated $Hg^{2+}$ complex compared to the $Au^+$ one, it should be informative to interest ourselves in clusters.

We should highlight here that the structures we optimized are different from those of Afaneh et al.[15] However, their goal differed from ours by the fact that they tried to reproduce the structure of the solvated mercury but with a limited number of water molecules. Therefore, their optimization procedure differs from ours. They started from a mercury cation solvated by 30 water molecules, optimized the structure, and then kept only water from the first or second solvation shell. If this approach allows getting a good idea of the mercury solvated structures, it presupposes that the mercury geometry is purely centered and that the mercury will accept as many waters as possible in its first hydration shell (up to 6). The transition we observed is therefore totally ignored.

To assess the existence of the transition of $[Hg]_n$ complexes, we compared the energy of different $[Hg]_6$ complexes (the results are exposed in Figure S6 and Table S1 in the Supporting Information). More importantly, we studied the relative stability of a centered form against a linear ("gold type") form for the $[Hg]_3$ complex (see Figure 8a and b) at several

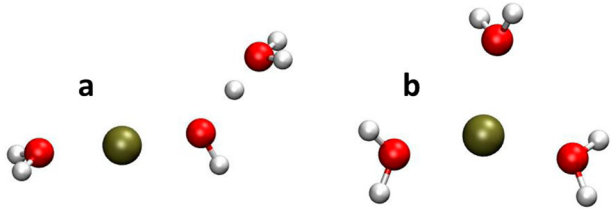


**Figure 8.** Visualization of ELF basins for "linear" or "gold type" complex (a) and the "centered" one (b).

levels of theory. If the linear form is more stable than the centered one (meaning $\Delta E$ negative), then there will necessarily be a transition from a gold type (linear) form to a more centered one, as it is known that the solvated $Hg^{2+}$ is seven-folded.[20,21,64] If the centered form is already the most stable one, then we can assess that there will not be any


dx.doi.org/10.1021/ct4006135 | J. Chem. Theory Comput. 2014, 10, 1900−1909

transition because the mercury will always try to have more than two water molecules in its first hydration shell.

A variety of DFT functionals (BLYP, PW91PW91, B3LYP, PBE0, and M06) and ab initio methods (HF, MP2, CCSD, CCSD(T)) were used, as well as different treatments of the relativistic effects: scalar treatment with SDD pseudopotential and two-component treatment with Douglass–Kroll–Hess theory (DKH2 and DKH4), as described in the Theoretical and Computational Methods section.

If modifying the basis sets (Figure 9a) does not influence the existence of a transition, the nature of the method used appears

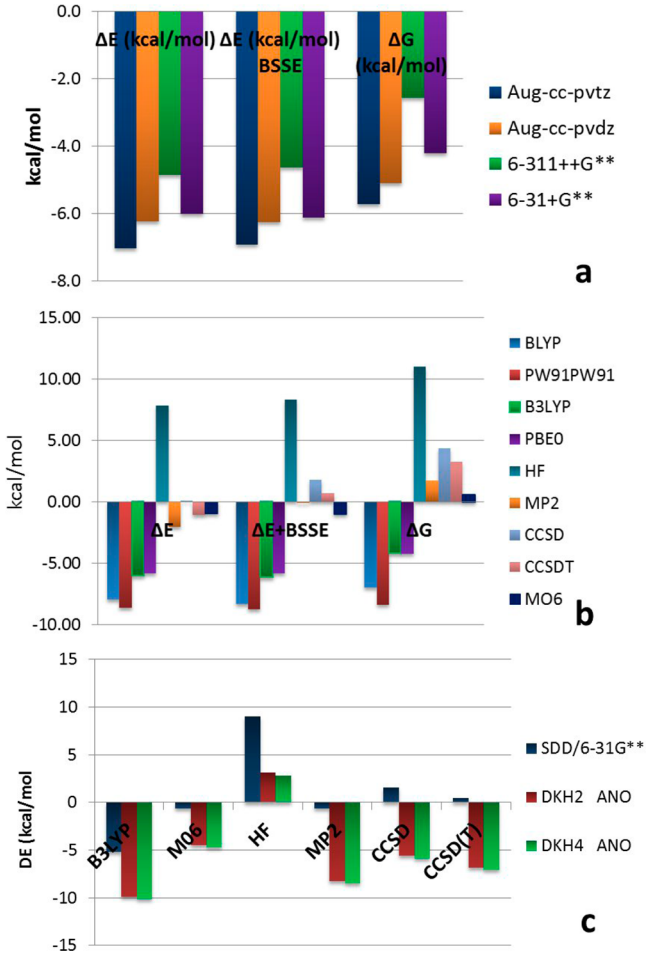


**Figure 9.** Difference of energy, energy + BSSE, and free energy between the linear and the centered complexes: $\Delta E = E_{\text{linear form}} - E_{\text{centered form}}$. (a) Using different basis sets and B3LYP; (b) using various levels of theory and the 6-31+G** basis set; (c) using various functionals and ab initio methods and for different treatments of relativistic effects.

to be very important (Figure 9b). Indeed, except for M06 that reproduces well MP2 relative energy, DFT functionals stabilize more the linear form contrary to ab initio methods that prefer rather the centered one. This is due to the correlation and dispersion treatments that are different in these two sets of methods. As no nondynamical correlation is to taken into account, we can consider the CCSD(T) method as a reference, and then no transition should be considered at this level of theory.

The use of the Douglas–Kroll level of theory that improves the treatment of the relativistic effects leads however to a stabilization of the linear form (Figure 9c). The latter appears finally more stable than the centered one, and the topological transition needs to be invoked again. The geometry of the solvated mercury cation appears therefore as a fragile equilibrium between correlation and relativity effects.

**Interaction between the $Hg^{2+}$ and Other Ligands.** The interactions between the various mercury ligands were studied so as to understand better the nature of the different forms of the mercury.[65] Figure 10 shows that the hardest ligand

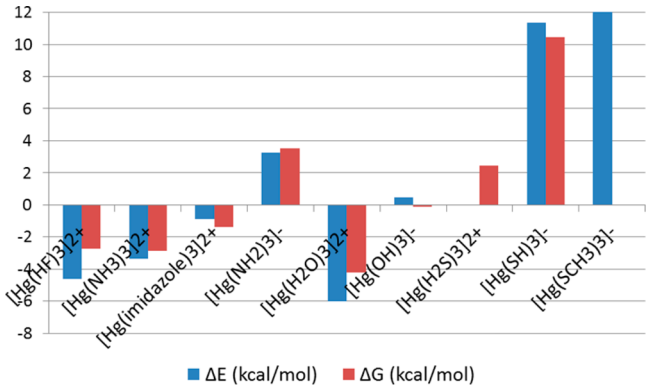


**Figure 10.** Energy and free energy differences between the linear and centered forms for the nine different ligands (HF, $NH_3$, imidazole, $NH_2^-$, $H_2O$, $OH^-$, $H_2S$, $HS^-$, and $CH_3S^-$) computed at the B3LYP/SDD/6-31+G** level of theory.

regarding the HSAB theory (HF, $NH_3$, or $H_2O$) are binding preferentially in a linear form corresponding to the pseudosoft complexed form of mercury. On the contrary, the softest ones ($H_2S$, $HS^-$, $CH_3S^-$, $OH^-$...) form preferentially centered (soft) complexes. The pseudosoft geometries exhibit a strong polarization and charge transfer effect: $E_1/E_2 < 1$ (see Theoretical and Computational Methods section for a definition of $E_1$ and $E_2$ and Table S2 for energy decomposition values). These properties had already been linked by Gourlaouen et al.[11] to the reduction of the energy of the $(n + 1)s^0$ orbital of the cation due to the relativistic effects. On the contrary, the soft centered form has $E_1/E_2 > 1$, which is characteristic of a state where relativistic effects play a minor role and, thus, correlation effects are predominant.

Then, the transition observed in mercury solvation structures appears to be dependent on the nature of the ligand considered. For a hard ligand, the pseudosoft form will be preferred and the transition will be observed, whereas for a soft one, the soft form will be adopted from the beginning.

Finally, the differences between mercury and gold cations' microsolvated geometries and, particularly, the existence of a transition in the solvation structure can now be explained in terms of importance of the relativistic effects. Relativity freezes the metal cation in a linear geometry (for gold and mercury). In gold, relativity is so important that correlation effects do not manage to reach the importance of relativistic ones, and the clusters remain in the linear type geometry whatever the number of water molecules. On the contrary, as relativity is smaller in mercury, correlation effects manage to reach the importance of relativistic ones. When they get higher, the geometry is then driven by correlation effects and the cation manages to accept more than two water molecules in its first hydration shell, which induces the topological transition. Overall, these results highlight the need for high level


dx.doi.org/10.1021/ct4006135 | J. Chem. Theory Comput. 2014, 10, 1900–1909

computation for mercury complexes. However, it appears that, if one should use a CCSD(T)/4-component reference level, the simpler B3LYP/SDD level gives fairly good results.

## 5. CONCLUSIONS AND PERSPECTIVES

The study of microsolvated complexes appears as a powerful model to understand the physics of the nucleation of water molecules around metal cations such as gold and mercury. In this contribution, we proposed an in depth study of such complexes using quantum interpretative techniques. Solvated structures as well as ELF topological analysis confirmed that the $Au^+$ only accepts two water molecules in its first hydration shell. However, it also interacts with other water molecules, further away, through weak interactions, as shown by NCI. Thus, the ELF analysis of $Au^+$ shows a peculiar aspect of its electronic structure in that the cation exhibits the capability of preorganizing its outer-shell core electrons (subvalence) into two half-spheres directed toward Au−O bonds and will then never modify it whatever the number of water molecules added. This behavior is not characteristic of a hard cation that splits its subvalence nor of a soft cation as it keeps it unchanged. We therefore decided to extend the usual description and to refer to $Au^+$ as a pseudosoft cation. A population analysis of the gold cation was also carried out on the $[Au]_n$ cluster using several levels of theories and methods. It seems necessary to use NBO or QTAIM population analysis with hybrid DFT calculation and at least a double-$\zeta$ basis set to model, accurately enough, gold charge. In such a case, gold can recover up to 0.4 $e^-$ and therefore have a charge of +0.6 $e^-$.

$Hg^{2+}$ microsolvation was shown to be similar to the $Au^+$ one for small clusters (less than eight water molecules); it only binds to two water molecules, and its subvalence is also two half-spheres directed toward Hg−O bonds. However, for larger clusters, a geometric and topological transition appears inducing the arrival of more than two water molecules in the first hydration shell of the cation and the modification of its subvalence topology. This transition can be followed looking at the different QTAIM distributed moments on the mercury or at the polarization and charge transfer energies as obtained from EDA computations. NCI analysis shows however that despite the fact that more than two water molecules bond the cation, it will still keep a "gold type" geometry as two of them, situated on each part of the cation, will remain more strongly bonded to it.

The existence of the transition was studied at several levels of treatment of the electronic correlation (HF, post-HF, and DFT methods) and relativistic effects (pseudopotential, DKH2, and DKH4), and the results point out their antagonist effects: if relativistic effects are predominant, then the mercury will behave like gold and have a similar subvalence; otherwise when electronic correlation effects are predominant, $Hg^{2+}$ behaves more like a soft cation, splitting additionally its subvalence.

The results presented here also highlight the interest of the synergetic use of several interpretative methods to study complex systems under the same philosophy as that for the results some of us presented for the reaction mechanism.[50] All of the different schemes used here (ELF, QTAIM, NCI, EDA...) have exposed different properties of the two cations that, gathered together, allowed a more detailed description of the systems that could be, for example, used for the design of next generation force fields, allowing larger systems to be tackled.[66]

## ■ ASSOCIATED CONTENT

### Supporting Information

Additional Tables and Figures can be found as Supporting Information. This material is available free of charge via the Internet at http://pubs.acs.org

## ■ AUTHOR INFORMATION


### Corresponding Author

*E-mail: jpp@lct.jussieu.fr.

### Present Address

[⊥]Scienomics, 17 square Edouard VII, 75009 Paris, France.


### Notes

The authors declare no competing financial interest.

## ■ ACKNOWLEDGMENTS

This work is partially supported by the National Institute of Health (W.Y. and R.C.; 5-R01-GM-061870).

## ■ REFERENCES


(1) Wilson, C. T. R. *Philos. Trans. R. Soc. London* **1897**, *189*, 265. Das Gupta, N. N.; Ghosh, S. K. *ReV. Mod. Phys.* **1946**, *18*, 225. Onianwa, P. C.; Odukoya, O. O.; Alabi, H. A. *Bull. Chem. Soc. Ethiop.* **2002**, *16*, 141. Aas, W.; Shao, M.; Jin, L.; Larssen, T.; Zhao, D.; Xiang, R.; Zhang, J.; Xiao, J.; Duan, L. *Atmos. Environ.* **2007**, *41*, 1706.

(2) Fuke, K.; Hashimoto, K.; Iwata, S. In *Advances in Chemical Physics*; John Wiley & Sons Inc: New York, 1999; Vol. *110*, p 431.

(3) Boening, D. W. *Chemosphere* **2000**, *40*, 1335.

(4) Gorin, D. J.; Toste, F. D. *Nature* **2007**, *446*, 395.

(5) (a) Poisson, L.; Lepetit, F.; Mestdagh, J. M.; Visticot, J. P. *J. Phys. Chem. A* **2002**, *106*, 5455. (b) Poisson, L.; Pradel, P.; Lepetit, F.; Reau, F.; Mestdagh, J. M.; Visticot, J. P. *Eur. Phys. J. D* **2001**, *14*, 89.

(6) (a) Orgel, L. E. *J. Chem. Soc.* **1958**, 4186. (b) Pyykkö, P. *Angew. Chem., Int. Ed.* **2004**, *43*, 4412. (c) Pyykkö, P. *Chem. Soc. Rev.* **2008**, *37*, 1967. (d) Xiong, X. G.; Xu, W. H.; Li, J.; Pyykkö, P. *Int. J. Mass Spectrom.* **2013**, *354*, 15−18.

(7) Reveles, J. U.; Calaminici, P.; Beltran, M. R.; Koster, A. M.; Khanna, S. N. *J. Am. Chem. Soc.* **2007**, *129*, 15565.

(8) Shepler, B. C.; Wright, A. D.; Balabanov, N. B.; Peterson, K. A. *J. Phys. Chem. A* **2007**, *111*, 11342.

(9) Hertwig, R. H.; Hrusak, J.; Schroder, D.; Koch, W.; Schwarz, H. *Chem. Phys. Lett.* **1995**, *236*, 194.

(10) Feller, D.; Glendening, E. D.; de Jong, W. A. *J. Chem. Phys.* **1999**, *110*, 1475.

(11) Gourlaouen, C.; Piquemal, J. P.; Saue, T.; Parisel, O. *J. Comput. Chem.* **2006**, *27*, 142.

(12) Cox, H.; Stace, A. J. *J. Am. Chem. Soc.* **2004**, *126*, 3939.

(13) Kraka, E.; Filatov, M.; Cremer, D. *Croat. Chem. Acta* **2009**, *82*, 233.

(14) Cremer, D.; Kraka, E.; Filatov, M. *ChemPhysChem* **2008**, *9*, 2510.

(15) Afaneh, A. T.; Schreckenbach, G.; Wang, F. *Theor. Chem. Acc.* **2012**, 131.

(16) Camellone, M. F.; Marx, D. *Phys. Chem. Chem. Phys.* **2012**, *14*, 937.

(17) Rode, B. M.; Schwenk, C. F.; Hofer, T. S.; Randolf, B. R. *Coord. Chem. Rev.* **2005**, *249*, 2993.

(18) Kritayakornupong, C.; Plankensteiner, K.; Rode, B. M. *Chem. Phys. Lett.* **2003**, *371*, 438.

(19) Kritayakornupong, C.; Rode, B. M. *J. Chem. Phys.* **2003**, *118*, 5065.

(20) D'Angelo, P.; Migliorati, V.; Mancini, G.; Barone, V.; Chillemi, G. *J. Chem. Phys.* **2008**, *128*, 6.

(21) Chillemi, G.; Mancini, G.; Sanna, N.; Barone, V.; Della Longa, S.; Benfatto, M.; Pavel, N. V.; D'Angelo, P. *J. Am. Chem. Soc.* **2007**, *129*, 5430.

(22) Maliarik, M.; Persson, I. *Magn. Reson. Chem.* **2005**, *43*, 835.

(23) Sobolev, O.; Cuello, G. J.; Roman-Ross, G.; Skipper, N. T.; Charlet, L. *J. Phys. Chem. A* **2007**, *111*, 5123.
(24) de Courcy, B.; Pedersen, L. G.; Parisel, O.; Gresh, N.; Silvi, B.; Pilmé, J.; Piquemal, J. P. *J. Chem. Theory Comput.* **2010**, *6*, 1048.
(25) Becke, A. D.; Edgecombe, K. E. *J. Chem. Phys.* **1990**, *92*, 5397.
(26) Silvi, B.; Savin, A. *Nature* **1994**, *371*, 683.
(27) Bagus, P. S.; Illas, F. *J. Chem. Phys.* **1992**, *96*, 8962.
(28) Johnson, E. R.; Keinan, S.; Mori-Sanchez, P.; Contreras-Garcia, J.; Cohen, A. J.; Yang, W. T. *J. Am. Chem. Soc.* **2010**, *132*, 6498.
(29) Contreras-Garcia, J.; Johnson, E. R.; Keinan, S.; Chaudret, R.; Piquemal, J.-P.; Beratan, D.; Yang, W. *J. Chem. Theory Comput.* **2011**, *7*, 625.
(30) Frisch, M. J.; Trucks, G. W.; Schlegel, H. B.; Scuseria, G. E.; Robb, M. A.; Cheeseman, J. R.; Scalmani, G.; Barone, V.; Mennucci, B.; Petersson, G. A.; Nakatsuji, H.; Caricato, M.; Li, X.; Hratchian, H. P.; Izmaylov, A. F.; Bloino, J.; Zheng, G.; Sonnenberg, J. L.; Hada, M.; Ehara, M.; Toyota, K.; Fukuda, R.; Hasegawa, J.; Ishida, M.; Nakajima, T.; Honda, Y.; Kitao, O.; Nakai, H.; Vreven, T.; Montgomery, J. A., Jr.; Peralta, J. E.; Ogliaro, F.; Bearpark, M.; Heyd, J. J.; Brothers, E.; Kudin, K. N.; Staroverov, V. N.; Kobayashi, R.; Normand, J.; Raghavachari, K.; Rendell, A.; Burant, J. C.; Iyengar, S. S.; Tomasi, J.; Cossi, M.; Rega, N.; Millam, N. J.; Klene, M.; Knox, J. E.; Cross, J. B.; Bakken, V.; Adamo, C.; Jaramillo, J.; Gomperts, R.; Stratmann, R. E.; Yazyev, O.; Austin, A. J.; Cammi, R.; Pomelli, C.; Ochterski, J. W.; Martin, R. L.; Morokuma, K.; Zakrzewski, V. G.; Voth, G. A.; Salvador, P.; Dannenberg, J. J.; Dapprich, S.; Daniels, A. D.; Farkas, Ö.; Foresman, J. B.; Ortiz, J. V.; Cioslowski, J.; Fox, D. J. *Gaussian 09*, revision D.01; Gaussian, Inc.: Wallingford, CT, 2009.
(31) Becke, A. D. *J. Chem. Phys.* **1993**, *98*, 5648.
(32) Lee, C. T.; Yang, W. T.; Parr, R. G. *Phys. Rev. B* **1988**, *37*, 785.
(33) Harihara, P.; Pople, J. A. *Theor. Chim. Acta* **1973**, *28*, 213.
(34) Dolg, M.; Stoll, H.; Preuss, H.; Pitzer, R. M. *J. Phys. Chem.* **1993**, *97*, 5852.
(35) (a) Perdew, J. P.; Burke, K.; Ernzerhof, M. *Phys. Rev. Lett.* **1996**, *77*, 3865. (b) Adamo, C.; Barone, V. *Chem. Phys. Lett.* **1997**, *274*, 242−250.
(36) Perdew, J. P.; Wang, Y. *Phys. Rev. B* **1992**, *45*, 13244.
(37) Krishnan, R.; Binkley, J. S.; Seeger, R.; Pople, J. A. *J. Chem. Phys.* **1980**, *72*, 650.
(38) Dunning, T. H. *J. Chem. Phys.* **1989**, *90*, 1007.
(39) Reiher, M. *Theor. Chem. Acc.* **2006**, *116*, 241.
(40) Reiher, M.; Wolf, A. *J. Chem. Phys.* **2004**, *121*, 10945.
(41) Reiher, M.; Wolf, A. *J. Chem. Phys.* **2004**, *121*, 2037.
(42) Mulliken, R. S. *J. Chem. Phys.* **1955**, *23*, 1833.
(43) Reed, A. E.; Weinhold, F. *J. Chem. Phys.* **1983**, *78*, 4066.
(44) Reed, A. E.; Weinstock, R. B.; Weinhold, F. *J. Chem. Phys.* **1985**, *83*, 735.
(45) Bader, R. F. W. *Atoms in Molecules: A Quantum Theory Oxford*; Oxford University Press: New York, 1990.
(46) Matta, C. F.; Boyd, R. J. Wiley-VCH: Weinheim, Germany, 2007.
(47) Noury, S.; Krokidis, X.; Fuster, F.; Silvi, B. *J. Comput. Chem.* **1999**, *23*, 597−604.
(48) (a) Popelier, P. L. A. *Atoms in Molecules: An Introduction*; Prentice-Hall: Harlow, U. K., 2000. (b) Popelier, P. L. A. *Mol. Phys.* **1996**, *87*, 1169. (c) Popelier, P. L. A.; Stone, A. J. *Mol. Phys.* **1994**, *82*, 411. (d) Popelier, P. L. A.; Joubert, L.; Kosov, D. S. *J. Phys. Chem. A* **2001**, *105*, 8254.
(49) Pilmé, J.; Piquemal, J. P. *J. Comput. Chem.* **2008**, *29*, 1440.
(50) Zhao, Y.; Truhlar, D. G. *Theor. Chem. Acc.* **2008**, *120*, 215.
(51) Hehre, W. J.; Stewart, R. F.; Pople, J. A. *J. Chem. Phys.* **1969**, *51*, 2657.
(52) Binkley, J. S.; Pople, J. A.; Hehre, W. J. *J. Am. Chem. Soc.* **1980**, *102*, 939.
(53) Godbout, N.; Salahub, D. R.; Andzelm, J.; Wimmer, E. *Can. J. Chem.* **1992**, *70*, 560.
(54) Gillespie, R. J.; Nyholm, R. S. Q. *Rev. Chem. Soc.* **1957**, *11*, 339.
(55) Chaudret, R.; Piquemal, J.-P.; Cisneros, G. A. *Phys. Chem. Chem. Phys.* **2011**, *13*, 11239.
(56) Fang, D.; Chaudret, R.; Piquemal, J.-P.; Cisneros, G. A. *J. Chem. Theory Comput.* **2013**, *9*, 2156.
(57) Gillet, N.; Chaudret, R.; Contreras-Garcia, J.; Yang, W.; Silvi, B.; Piquemal, J.-P. *J. Chem. Theory Comput.* **2012**, *8*, 3993.
(58) (a) Piquemal, J.-P.; Marquez, A.; Parisel, O.; Giessner-Prettre, C. *J. Comput. Chem.* **2005**, *26*, 1052. (b) Gourlaouen, C.; Piquemal, J.-P.; Parisel, O. J. *Chem. Phys.* **2006**, *124*, 174311. (c) Gourlaouen, C.; Parisel, O.; Piquemal, J.-.P *Chem. Phys. Lett.* **2009**, *469*, 38. (d) Marjolin, A.; Gourlaouen, C.; Clavaguera, C.; Dognon, J.-P.; Piquemal, J.-P. *Chem. Phys. Lett.* **2013**, *563*, 25.
(59) Dupuis, M.; Marquez, A.; Davidson, E. R. *HONDO95.3, Quantum Chemistry Program Exchange QCPE*; Indiana University: Bloomington, IN.
(60) Lee, H. M.; Min, S. K.; Lee, E. C.; Min, J. H.; Odde, S.; Kim, K. S. *J. Chem. Phys.* **2005**, *122*, 10.
(61) Slee, T.; Larouche, A.; Bader, R. F. W. *J. Phys. Chem.* **1988**, *92*, 6219.
(62) Cohen, A. J.; Mori-Sanchez, P.; Yang, W. T. *Phys. Rev. B* **2008**, *77*, 6.
(63) Mori-Sanchez, P.; Cohen, A. J.; Yang, W. T. *Phys. Rev. Lett.* **2008**, *100*, 4.
(64) Mancini, G.; Sanna, N.; Barone, V.; Migliorati, V.; D'Angelo, P.; Chillemi, G. *J. Phys. Chem. B* **2008**, *112*, 4694.
(65) (a) Riccardi, D.; Guo, H. B.; Parks, J. M.; Gu, B.; Summers, A. O.; Miller, S. M.; Liang, L.; Smith, J. C. *J. Phys. Chem. Lett.* **2013**, *4*, 2317. (b) Riccardi, D.; Guo, H. B.; Parks, J. M.; Gu, B.; Summers, A. O.; Miller, S. M.; Liang, L.; Smith, C. *J. Chem. Theory Comput.* **2013**, *9*, 555.
(66) (a) Gresh, N.; Cisneros, G. A.; Darden, T. A.; Piquemal, J.-P. *J. Chem. Theory Comput.* **2007**, *3*, 1960. (b) Piquemal, J.-P.; Perera, L.; Cisneros, G. A.; Ren, P. Y.; Pedersen, L. G.; Darden, T. A. *J. Chem. Phys.* **2006**, *125*, 054511. (c) Wu, J.; Piquemal, J.-P.; Chaudret, R.; Reinhardt, P.; Ren, P. Y. *J. Chem. Theory Comput.* **2010**, *6*, 2059. (d) Devereux, M.; van Severen, M.-C.; Parisel, O.; Piquemal, J.-P.; Gresh, N. *J. Chem. Theory Comput.* **2011**, *7*, 138. (e) Marjolin, A.; Gourlaouen, C.; Clavaguera, C.; Gresh, N.; Ren, P. Y.; Wu, J.; Dognon, J.-P.; Piquemal, J.-P. *Theor. Chem. Acc.* **2012**, *131*, 1198.